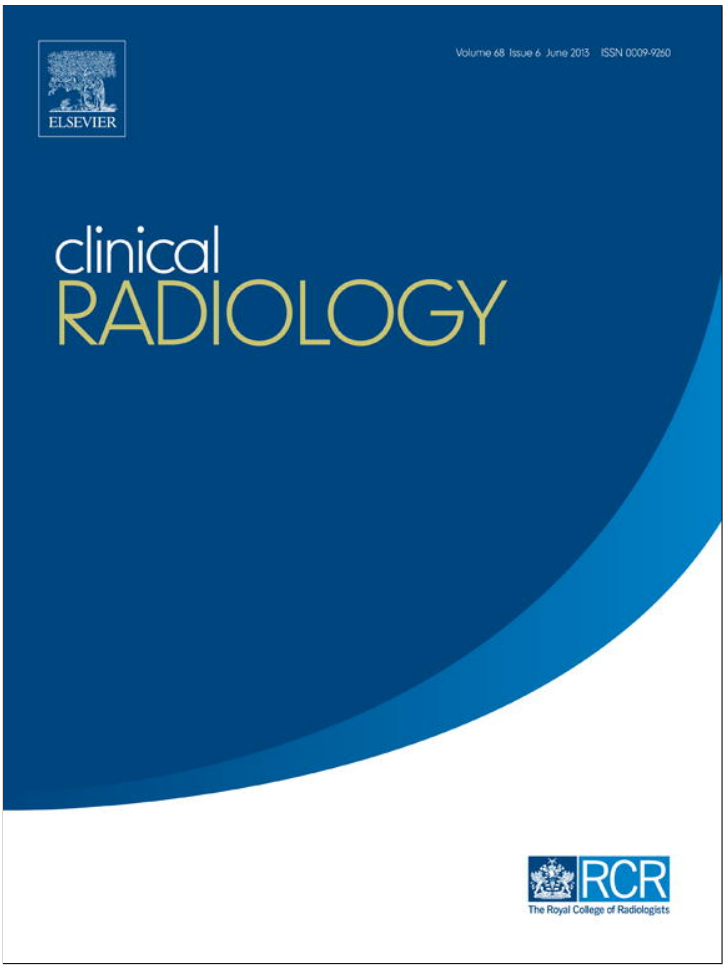

Clinical Radiology 68 (2013) e301–e308

Contents lists available at SciVerse ScienceDirect

Clinical Radiology

journal homepage: www.clinicalradiologyonline.net

# Small solid renal masses: Characterization by diffusion-weighted MRI at 3 T

F. Agnello [a,*], C. Roy [a], G. Bazille [a], M. Galia [b], M. Midiri [b], T. Charles [c], H. Lang [c]

[a] Department of Radiology B, Universitary Hospital of Strasbourg, Strasbourg, France
[b] Department of Radiology, University of Palermo, Palermo, Italy
[c] Department of Urology, Universitary Hospital of Strasbourg, Strasbourg, France

ARTICLE INFORMATION

*Article history:*
Received 11 September 2012
Received in revised form
23 December 2012
Accepted 2 January 2013

AIM: To describe the appearance of small solid renal lesions (≤3 cm) on diffusion-weighted magnetic resonance imaging (MRI) and to determine whether ADC measurements may help to differentiate benign from malignant small solid renal masses.

METHODS AND MATERIALS: Thirty-five patients with 47 small renal masses (23 malignant, 24 benign) who underwent 3 T MRI of the kidney using diffusion-weighted sequences (b values of 0 and 1000 s/mm$^2$) were retrospectively evaluated. Qualitative and quantitative analysis of diffusion-weighted images was performed.

RESULTS: Most lesions were hyperintense to kidney on high b-value diffusion-weighted images and hypointense on apparent diffusion coefficient (ADC) map. The mean ADC of the lesions was significantly lower than that of kidney (1.22 ± 0.3 versus 1.85 ± 0.12 mm$^2$/s; $p < 0.005$). The mean ADC was significantly different between renal cell carcinomas (1.2 ± 0.01 mm$^2$/s), metastases (1.25 ± 0.04 mm$^2$/s), angiomyolipoma (1.07 ± 0.3 mm$^2$/s) and oncocytomas (1.56 ± 0.08 mm$^2$/s; $p < 0.05$). The mean ADC of clear cell renal cell carcinomas was significantly different from that of non-clear cell renal cell carcinomas (1.38 ± 0.34 versus 0.83 ± 0.34 mm$^2$/s; $p < 0.005$). No significant difference was found between mean ADC of fat containing and minimal fat angiomyolipomas (1.06 ± 0.48 versus 1.11 ± 0.33 mm$^2$/s).

CONCLUSION: Small solid renal masses are hyperintense on high b value and have different ADC values.



## Introduction

The widespread use of ultrasound and computed tomography (CT) in daily practice for various abdominal complaints allows for increased incidental discovery of small solid renal masses (≤3 cm) in patients with no urinary tract symptoms.[1] The majority of these masses are malignant, but benign tumours account for 20–25% of all such masses.[2,3] As a consequence, most renal cell carcinomas (RCC) are now incidentally discovered.[4] Differentiation of benign from malignant lesions is crucial in deciding on a therapeutic approach.[5] Indeed, small malignant renal masses are usually surgically removed or treated with minimally invasive percutaneous procedures,[6] whereas benign renal masses are managed conservatively. Small solid renal masses are known to be difficult to characterize, except for angiomyolipoma (AML) with large macroscopic fatty tissue.[7] Currently, characterization of renal masses is based primarily on their appearance on unenhanced CT and magnetic resonance imaging (MRI; i.e., the presence of macroscopic fat) and the degree of enhancement at CT and MRI.[8–10] Central stellate fibrosis is seen in only 10% of

* Guarantor and correspondent: F. Agnello. Present address: Diagnostic and Therapeutic Services, Mediterranean Institute for Transplantation and Advanced Specialized Therapies (IsMETT), University of Pittsburgh Medical Center Italy, Via Tricomi 1, 90100 Palermo, Italy. Tel.: +39 339 46 73 894.
*E-mail address:* fra.agnello@libero.it (F. Agnello).

0009-9260/$ – see front matter © 2013 The Royal College of Radiologists. Published by Elsevier Ltd. All rights reserved.
http://dx.doi.org/10.1016/j.crad.2013.01.002

oncocytomas if the lesion is < 3 cm.[11] Several diagnostic clues have been suggested. For example, segmental enhancement inversion in the corticomedullary and excretory phases suggests a diagnosis of oncocytoma,[12] whereas the presence of an angular interface with the renal parenchyma is considered a strong predictor of benignity in an exophytic renal mass.[13] However, conventional imaging methods are not specific enough for differentiating malignant from benign small solid masses[6,9,14–17]; therefore, percutaneous renal biopsy is usually recommended to correctly characterize small renal lesions.[6] However, this procedure has some limitations: it is not universally available, and although uncommon, procedural complications and potential sampling errors can occur.

Several recent studies have shown that diffusion-weighted imaging (DWI) may help to characterize renal lesions and to differentiate benign from malignant renal masses.[18–23] However, to the authors' knowledge, the value of DWI has not specifically been studied to characterize small solid renal masses. Therefore, the purpose of the present study was to describe the appearance of small solid renal masses on DWI images and to determine whether apparent diffusion coefficient (ADC) measurements can aid in differentiating benign from malignant small solid renal masses.

## Materials and methods

### *Study population*

The Institutional Review Board approved this study and informed patient consent was waived.

The electronic database of our department (Department of Radiology B, Universitary Hospital of Strasbourg, Strasbourg, France) was retrospectively reviewed for all MRI examinations of the kidney between April 2008 and December 2011 to select patients who presented at least one solid renal lesion measuring 1–3 cm in maximum diameter. Lesions of <1 cm in size were excluded in order to avoid errors due to partial volume effect. A total of 65 patients were identified. From this initial group of 65, 30 patients were excluded for the following reasons: presence of infarction, haemorrhage, or infection that could mimic a solid renal neoplasm ($n = 15$); no reference standard ($n = 10$); and MRI artefacts that made the examination non-diagnostic ($n = 5$). The remaining 35 patients (mean age 61.6 years; range 27–88 years) were included in the study. There were 19 men (mean age 60.5 years; range 27–88 years) and 16 women (mean age 61.5 years; range 27–77 years). All patients had a glomerular filtration rate of 30–60 ml/min/m$^2$. Three patients had tuberous sclerosis. No patient had von Hippel–Lindau syndrome. In the presence of multiple renal lesions, a maximum of two was selected. Thus, 35 patients with 47 lesions were evaluated.

### *Data collection and reference standard*

The standard of reference was the pathological analysis obtained from ultrasound-guided biopsy with an 18-G automated device and three cores under 1% lidocaine local anaesthesia or surgical resection. In fat-containing AMLs for which histopathological examination was not performed, the diagnosis was established by using known published criteria. These included (a) T1 tiny hyperintense spots; (b) signal loss on fat-saturated images; (c) presence of an ink artefact on chemical shift sequences; and (d) no change over time for at least 15 months on MRI follow-up.[8]

### *Imaging protocol*

All examinations were performed using a 3 T MRI unit (Achieva, Philips Medical Systems, Best, The Netherlands) using a dedicated abdominal phased-array coil with 32 coils. The standard protocol included the following sequences acquired in an axial plane: T2-weighted turbo spin-echo, fat-saturated T2-weighted turbo spin-echo, T1-weighted dual gradient-recalled echo, and diffusion-weighted and three-dimensional fat-saturated dynamic gadolinium-enhanced T1-weighted gradient-recalled echo.

Dynamic contrast-enhanced images were acquired before and after the injection of 0.1 mmol gadobenate dimeglumine (Multihance, Bracco, Milan, Italy) per kilogram of body weight followed by a 20 ml saline flush, both at 2 ml/s using a power injector (Spectris; Medrad, Pittsburgh, PA, USA). The scanning delays were 50, 90, 120, and 180 s after the injection of the contrast material.

A single-shot DWI was obtained before contrast material administration using echo-planar imaging with a pair of motion-probing gradients along three orthogonal axes, chemical shift selective fat-saturation technique, two b values (0 and 1000 s/mm$^2$), and free breathing. DWI images were reconstructed for each pixel by using a dedicated post-processing software (diffusion calculation, Achieva, Version 6.2, Philips Medical Systems), and an ADC map was automatically generated to obtain a mono-exponential fit of the data. MRI parameters are detailed in Table 1.

### *Imaging analysis*

Images were retrospectively and independently evaluated on the workstation of the MRI unit by two radiologists: a fellow involved in this field (F.A.) and an experienced radiologist with 15 years of experience in abdominal imaging (C.R.). The readers were unaware of the final diagnosis. Disagreements were discussed and resolved in consensus. DWI images were evaluated first qualitatively and then quantitatively.

### *DWI qualitative analysis*

Lesions were evaluated on DWI images with b value of 0 and 1000 s/mm$^2$ and on the ADC map on the basis of signal intensity (SI) relative to the surrounding kidney and visual degree of SI change with increasing b value. The SI of the lesions relative to the kidney was classified into the following categories: hyperintense, isointense, and hypointense, compared with the surrounding kidney. Visual degree of SI change with increasing b value was classified in the following categories: increasing, similar, or decreasing.

**Table 1**
Magnetic resonance imaging (MRI) protocol.

| Sequence | T2-weighted TSE | T2-weighted TSE | T1-weighted dual GRE | DW imaging | T1-weighted 3D GRE |
|---|---|---|---|---|---|
| Fat suppression | No | Yes | No | Yes | Yes |
| TR/TE (ms) | 2153/80 | 1927/80 | 10/2.3 | 7099/53 | 3.4/1.7 |
| Flip angle (degrees) | 90 | 90 | 15 | 90 | 10 |
| Matrix | 320 × 256 | 321 × 268 | 252 × 188 | 96 × 94 | 252 × 250 |
| Field of view (mm) | 370 | 370 | 370 | 340 | 370 |
| Section thickness (mm) | 5 | 5 | 5 | 5 | 4 |
| Section gap (mm) | 0.5 | 0.5 | 0.5 | – | – |
| Acquisition time (s) | 58 | 60 | 76 | 120 | 19 |

TSE, turbo spin echo; GRE, gradient-recalled echo; DW, diffusion-weighted; 3D, three-dimensional; TE, echo time; TR, repetition time.

### *DWI quantitative analysis*

The mean ADC value was calculated by manually placing a round or elliptical region of interest (ROI) encompassing the whole area of the suspected zone on the ADC map. Care was taken to avoid lesion margins in the ROI in order to minimize partial volume effects. The mean size of the ROIs was 3.8 ± 0.6 $cm^2$. One ROI of at least 1 $cm^2$ (mean 1.1 ± 0.4 $cm^2$; range 1–1.8 $cm^2$) was placed in the adjacent renal parenchyma, at the level of the cortico-medullary junction.

### *Statistical analysis*

Papillary, chromophobic, and indeterminate RCCs were combined into one group called non-clear cell (NCC) RCCs because of the small number of patients. The ADC was compared among the lesions and the kidney (Mann–Whitney *U*-test), among the different types of lesions (Kruskal–Wallis test), among clear cell (CC) RCCs and NCC RCCs (Student's *t*-test), and among fat-containing AMLs and minimal fat AMLs (Student's *t*-test). CC RCCs and NCC RCCs were also analysed as two independent types of lesions and the mean ADC among CC RCCs, NCC RCCs, metastases, AMLs, and oncocytomas were compared using the Kruskal–Wallis test. A *p*-value of less than 0.05 was considered the threshold for statistical significance. Receiver operating characteristic (ROC) analysis was done to evaluate the diagnostic performance of the ADC for differentiating CC RCCs from NCC RCCs, and from AMLs and oncocytomas, and for differentiating AMLs from oncocytomas. The optimum cut-off point was determined as the value that best discriminated between the types and subtypes in terms of maximum sensitivity and specificity.

## Results

### *Lesion characteristics*

The final study population comprised 47 lesions (mean diameter 2.1 cm; range 1.1–3 cm). Twenty-three of the 47 (49%) lesions were malignant (mean diameter 2.1 cm; range 1.2–3 cm) and 24/47 (51%) lesions were benign (mean diameter 2.1 cm; range 1.1–3 cm). Eighteen lesions were located in the upper part of the kidney, 17 lesions were located in the middle part, and 12 lesions were located in the lower part. Malignant lesions included 19 RCCs (mean diameter 2.2 cm; range 1.2–3 cm) and four metastases (mean diameter 1.4 cm; range 1.3–1.6 cm). The primary site of origin of metastases was lung adenocarcinoma. RCCs included 13 CC RCCs (mean diameter 2.2 cm; range 1.3–3 cm) and six NCC RCCs (mean diameter 2.3 cm; range 1.2–3 cm). NCC RCCs included three papillary RCCs, one chromophobic RCC, and two indeterminate RCCs. Benign lesions included 17 AMLs (mean diameter 2 cm; range 1.1–3 cm) and seven oncocytomas (mean diameter 2.5 cm; range 1.8–3 cm). AMLs included nine fat-containing AMLs (mean diameter 20.6 cm; range 1.1–3 cm) and eight minimal fat AMLs (mean diameter 2 cm; range 1.2–3 cm). The final diagnosis was obtained by surgical resection [10 RCCs (six CC RCCs, four NCC RCCs), five oncocytomas, four AMLs (one fat-containing AML, three minimal fat AMLs)], core-biopsy [nine RCCs (seven CC RCCs, two NCC RCCs), four metastases, two oncocytomas, five AMLs (five minimal fat AMLs)] and typical MRI appearance in conjunction with stability in lesion size for at least 15 months (eight fat-containing AMLs).

### *DWI qualitative imaging analysis*

Results of the qualitative analysis are shown in Table 2. The image quality was quite good for each case. On these images, most lesions were hypointense compared with the kidney on b 0 s/$mm^2$, with an increase of signal intensity on b 1000 s/$mm^2$ (Figs 5 and 6), whereas only one oncocytoma was strongly hyperintense on b 0 s/$mm^2$ with a decrease of signal intensity on b 1000 s/$mm^2$ because of a large central scar. Except for one CC RCC and one oncocytoma that showed a moderate hyperintensity, all lesions were hypointense on the ADC map.

### *DWI quantitative imaging analysis*

Mean ADC values of the lesions were significantly lower than those of the kidney [1.22 ± 0.3 (range 0.76–1.90) versus 1.85 ± 0.12 (range 1.38–2.13); $p < 0.005$, Mann–Whitney test; Fig 1]. The mean ADC was significantly different among RCCs (1.2 ± 0.01 $mm^2$/s; range 0.76–1.73), metastases (1.25 ± 0.04 $mm^2$/s; range 1.1–1.57), AMLs (1.07 ± 0.3 $mm^2$/s; range 0.85–1.28), and oncocytomas (1.56 ± 0.08 $mm^2$/s; range 1.1–1.96; $p < 0.01$,

**Table 2**
Signal intensity of the lesions on DW images and ADC map.

| Lesion type | b 0 seconds/mm$^2$ | | | b 1000 seconds/mm$^2$ | | | SI change at increasing b values | | | ADC map | | |
|---|---|---|---|---|---|---|---|---|---|---|---|---|
| | Hyper | Iso | Hypo | Hyper | Iso | Hypo | Increased | Stable | Decreased | Hyper | Iso | Hypo |
| Malignant lesion | 4/23 (17) | 0 | 19/23 (83) | 21/23 (91) | 1/23 (4) | 1/23 (4) | 20/23 (87) | 3/23 (13) | 0 | 1/23 (4) | 0 | 22/23 (96) |
| RCCs | 4/19 (21) | 0 | 15/19 (79) | 17/19 (90) | 1/19 (5) | 1/19 (5) | 16/19 (84) | 3/19 (16) | 0 | 1/19 (5) | 0 | 18/19 (95) |
| CC RCCs | 4/13 (30) | 0 | 9/13 (70) | 11/13 (84) | 1/13 (8) | 1/13 (8) | 10/13 (77) | 3/13 (23) | 0 | 1/13 (8) | 0 | 12/13 (92) |
| NCC RCCs | 0 | 0 | 6/6 (100) | 6/6 (100) | 0 | 0 | 6/6 (100) | 0 | 0 | 0 | 0 | 6/6 (100) |
| Met | 0 | 0 | 4/4 (100) | 4/4 (100) | 0 | 0 | 4/4 (100) | 0 | 0 | 0 | 0 | 4/4 (100) |
| Benign lesions | 2/24 (8) | 2/24 (8) | 20/24 (82) | 22/24 (92) | 0 | 2/24 (8) | 22/24 (92) | 1/24 (4) | 1/24 (4) | 1/24 (4) | 1/24 (4) | 22/24 (92) |
| AMLs | 0 | 1/17 (6) | 16/17 (94) | 15/17 (88) | 0 | 2/17 (12) | 17/17 (100) | 0 | 0 | 0 | 0 | 17/17 (100) |
| FC AMLs | 0 | 0 | 9/9 (100) | 7/9 (78) | 0 | 2/9 (22) | 9/9 (100) | 0 | 0 | 0 | 0 | 9/9 (100) |
| MF AMLs | 0 | 1/8 (12) | 7/8 (88) | 8/8 (100) | 0 | 0 | 8/8 (100) | 0 | 0 | 0 | 0 | 8/8 (100) |
| Onc | 2/7 (28) | 1/7 (14) | 4/7 (58) | 7/7 (100) | 0 | 0 | 5/7 (72) | 1/7 (14) | 1/7 (14) | 1/7 (14) | 1/7 (14) | 5/7 (72) |

Data are numbers of lesions. Data in parentheses are percentages.
SI, signal intensity; hyper, hyperintense; iso, isointense; hypo, hypointense; RCCs, renal cell carcinomas; CC RCCs, clear cell type renal cell carcinomas; NCC RCCs, non-clear cell type renal cell carcinomas; met, metastases; AMLs, angiomyolipomas; FC AMLs, fat containing angiomyolipomas; MF AMLs, minimal fat angiomyolipomas; onc, oncocytomas.

Kruskal–Wallis test; Fig 2). There was a significant difference between mean ADC of CC RCCs (1.38 ± 0.34 mm$^2$/s; range 1.04–1.73) and NCC RCCs (0.83 ± 0.34 mm$^2$/s; range 0.76–1.01; $p < 0.005$, Student's *t*-test), whereas no significant difference was found between mean ADC of fat-containing AMLs (1.06 ± 0.48 mm$^2$/s, range 0.86–1.28) and minimal fat AMLs (1.11 ± 0.33 mm$^2$/s; range 1.04–1.22; $p = 0.22$, Student's *t*-test; Fig 3). Therefore, CC RCCs and NCC RCCs were analysed as two independent types of lesions; the mean ADC was significantly different among CC RCCs, NCC RCCs, metastases, AMLs, and oncocytomas ($p < 0.01$, Kruskal–Wallis test; Fig 4). The mean ADC value of CC RCCs was higher than that of AMLs, NCC RCCs and metastases, and was lower than that of oncocytomas. The best cut-off ADC values for differentiating CC RCCs from NCC RCCs, AMLs and oncocytomas were 1.2 mm$^2$/s (AUC = 1.00; $p = 0.00$; 100% sensitivity, 100% specificity); 1.12 mm$^2$/s (AUC = 0.82; $p < 0.001$; 88% sensitivity, 69% specificity) and 1.73 mm$^2$/s (AUC = 0.71; $p = 0.21$; 100% sensitivity, 60% specificity), respectively. The best cut-off ADC value for differentiating AMLs from oncocytomas was 1.21 mm$^2$/s (AUC = 0.922; $p < 0.0001$; 86% sensitivity, 88% specificity).

## Discussion

The present study shows that small solid renal masses with different tissue compositions have different apparent water diffusion, suggesting that DWI can be used as a non-invasive procedure to characterize small solid renal masses. In addition, this sequence can be obtained within a relatively short acquisition time and cannot be considered time consuming. Few studies have been performed to differentiate renal lesions using the ADC value.[12,19–24] These studies showed that oncocytomas had a higher ADC value than RCCs, whereas AMLs had a lower ADC value.[19–21] In addition, a recent study by Wang et al.[20] indicated that CC RCCs had a higher mean ADC value than NCC RCCs. However, to the authors' knowledge, no previous study has specifically analysed the utility of DWI for the characterization of small solid renal masses defined as ≤3 cm in maximum diameter. Similar to other reports, in the present series,

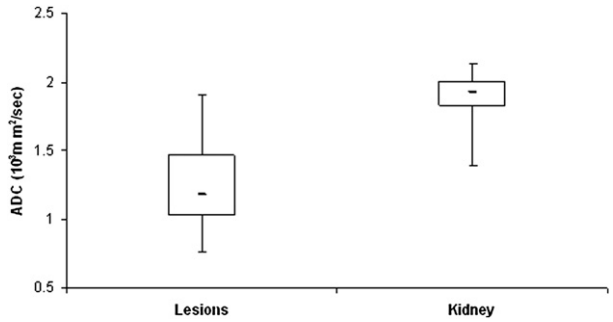


**Figure 1** Box-and-whisker plot of ADC values of renal lesions and uninvolved renal parenchyma. Horizontal line in each box is the median ADC value. Upper and lower margins of the box represent 75th and 25th percentile of values, respectively. Whiskers give range of values.

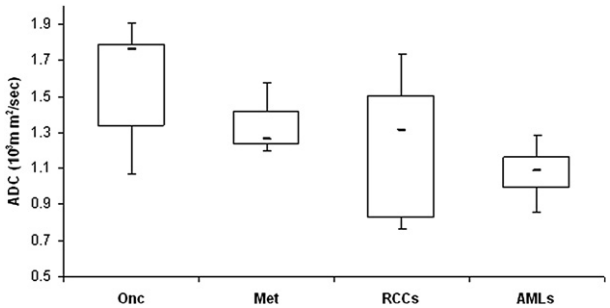


**Figure 2** Box-and-whisker plot of ADC values of oncocytomas (onc.), metastases (met), RCCs, and AMLs. Horizontal line in each box is the median ADC value. Upper and lower margins of the box represent 75th and 25th percentile of values, respectively. Whiskers give range of values.

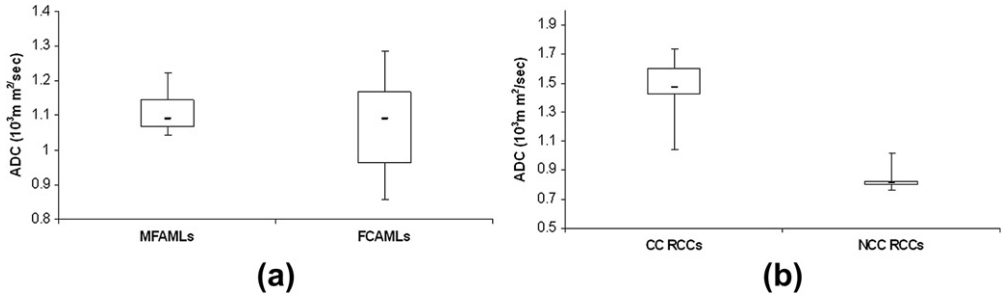


**Figure 3** Box-and-whisker plot distribution of ADC values of AML subtypes (a) and RCC subtypes (b). Horizontal line in each box is the median ADC value. Upper and lower margins of the box represent 75th and 25th percentile of values, respectively. Whiskers give range of values.

malignant lesions, such as RCCs and metastases had intermediate ADC values between those of AMLs and oncocytomas.[22,24] These results can be explained by the different histological architecture of these masses, as ADCs reflect the combined effects of capillary perfusion and diffusion.[25] AMLs contain varying amounts of fatty, angiomatous, and myomatous components, with an interstitial stroma that reduces water diffusion.[21,26] Oncocytomas are composed of eosinophilic cells (oncocytes) arranged in a variety of growth patterns, with a central fibrotic scar containing compressed blood vessels.[8] RCCs are a heterogeneous group of tumours characterized by different genetic and molecular abnormalities.[20] Four main subtypes of RCCs are described in the literature: clear cell, papillary, chromophobic, and indeterminate.[27] An accurate differentiation of these subtypes is crucial because CC RCCs are associated with a poorer prognosis than NCC RCCs, with the exception of indeterminate RCCs, which are less frequent than other subtypes.[22,28] In the present study, NCC RCCs had a lower ADC value than CC RCCs. A threshold value of 1.2 $mm^2/s$ allowed a differential diagnosis with high sensitivity and specificity. This can be explained by the different histological architecture of CC RCCs and NCC RCCs, as the latter contain small vessels without arterio-venous shunts.[27] A decreased perfusion could partially explain the decreased ADC. Contrary to other reports, in the present series, NCC RCCs had a mean ADC value that was lower than that of other small renal masses, AMLs included. In the literature,

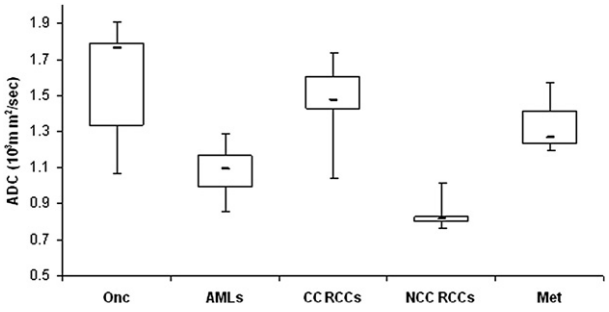


**Figure 4** Box-and-whisker plot of ADC values of oncocytomas (onc), AMLs, CC RCCs, NCC RCCs, and metastases (met). Horizontal line in each box is the median ADC value. Upper and lower margins of the box represent 75th and 25th percentile of values, respectively. Whiskers give range of values.

there is no consensus on the optimal b-value to be used at DWI.[20,21] High b-values increase diffusion weighting and, in theory, tumour detection, especially at 3 T. The ADC value is potentially an objective mean, but despite there being no official cut-off for tumours, the value of 1000 $mm^2/s$ seems a reasonable threshold. It is unclear why there is a discrepancy between the present observations and previous reports. However, if the present findings were to be confirmed in a larger series, it could be extremely important diagnostically. In view of findings of Zhang et al.,[29] it can be hypothesized that, because the main drawback of DWI is the lack of standardization, the variability of ADC values can probably be explained by differences in b values, coil systems, breath-hold versus free breathing, and field strengths used for MRI. Another interesting finding of the present study is the absence of a significant difference in mean ADC between fat-containing AMLs and minimal fat AMLs. Fat-containing AMLs can be easily identified with conventional MRI sequences,[8] but the present results indicate that DWI can be an interesting sequence to suggest a benign lesion in the case of minimal fat AMLs. However, it should be noted that overlap among ADC values between small solid renal masses was observed in the present series. This limits the applicability of ADC measurements for lesion characterization. For this reason, DWI could not be used as a standalone sequence for the characterization of small renal masses, and ADC values should be concurrently interpreted with all available images to avoid misinterpretation.

The present study shows that small renal masses have a lower ADC than the normal surrounding parenchyma ($1.22 \pm 0.27$ versus $1.85 \pm 0.12$). These results are in agreement with a study by Cova et al.,[24] who found higher ADC values in renal parenchyma compared with solid renal lesions ($2.19 \pm 0.17$ versus $1.55 \pm 0.2$).

A qualitative analysis of the lesions on DW images and ADC map was also performed. The present study demonstrates that almost all small solid renal masses show high signal intensity on higher b values and low signal intensity on the ADC map, when compared with normal renal parenchyma. Thus, the visual evaluation of DWI images is pertinent because of the high contrast with the surrounding parenchyma, and can be useful for the detection of small renal masses. These observations corroborate the results of a recent study by Blackledge et al.[30] on lesion detection with

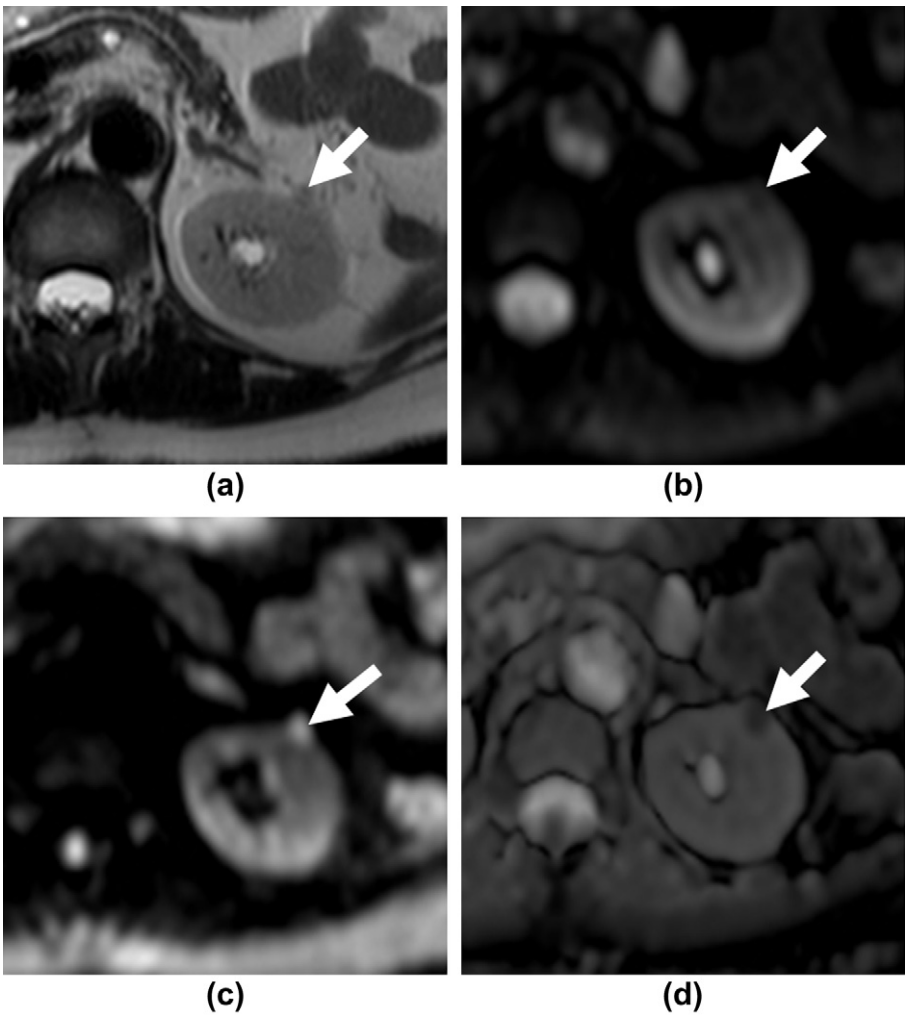


**Figure 5** CC RRC in a 73-year-old man. (a) Axial T2-weighted image shows a heterogeneously hyperintense lesion due to some hyperintense areas. (b, c) Axial DWI images with b values of 0 (b) and 1000 (c) s/mm$^2$: the lesion is heterogeneously hypointense at b0 s/mm$^2$ and heterogeneously hyperintense at b 1000 s/mm$^2$. Areas with increase in signal intensity at b 1000 indicate restricted diffusion. (d) Corresponding ADC map shows a heterogeneously hypointense lesion compared with kidney. Lesion ADC is $1.43 \times 10^{-3}$ mm$^2$/s. Kidney ADC is $1.95 \times 10^{-3}$ mm$^2$/s.

high b values DWI.[30] In addition, visual assessment is useful in differentiating solid from cystic lesions. Of note, in the present series, two AMLs were hypointense on b 0 and b 1000, though they showed a mild increase in signal intensity with increasing b value. This could be related to the fact that restriction of diffusion may not be sufficient to make the lesions hyperintense to kidney at high b value. Furthermore, as DWI is actually part of the routine MRI protocol in many centres, radiologists should keep in mind that most solid benign lesions are hyperintense at high b values and that hypointensity on the ADC map is not imperatively associated with malignancy.

The present study had several limitations. First, the number of lesions was relatively small in each group and subgroup. Moreover, there was a potential selection bias in the study, with 10 patients excluded because they had a small renal mass, but no sufficient confirmation of the nature of the lesion (i.e., lack of reference standard). Therefore, the present findings need to be confirmed in larger series. Second, pseudo-lesions (e.g., infarction, haemorrhage, or infection) were not evaluated in the study, which limits the ability to assess false-positive findings. Third, a mono-exponential assessment of ADC was used and, therefore, physiological processes, such as pure diffusion of water molecules and perfusion, may affect the estimation of ADC. A bi-exponential model based on multiple b value measurements is known to be better for ADC measurements. However, this latter solution is not practical in clinical use.[29] Last, because of the aim of the study, diffusion-weighted sequences were not compared with T2-weighted sequences and contrast-enhanced T1-weighted sequences for the detection and characterization of small solid renal lesions.

In conclusion, small solid renal masses with different tissue composition were found to be hyperintense on high b values and have different ADC values. This suggests that DWI can provide supporting information for detecting and characterizing small solid renal masses. However, as some

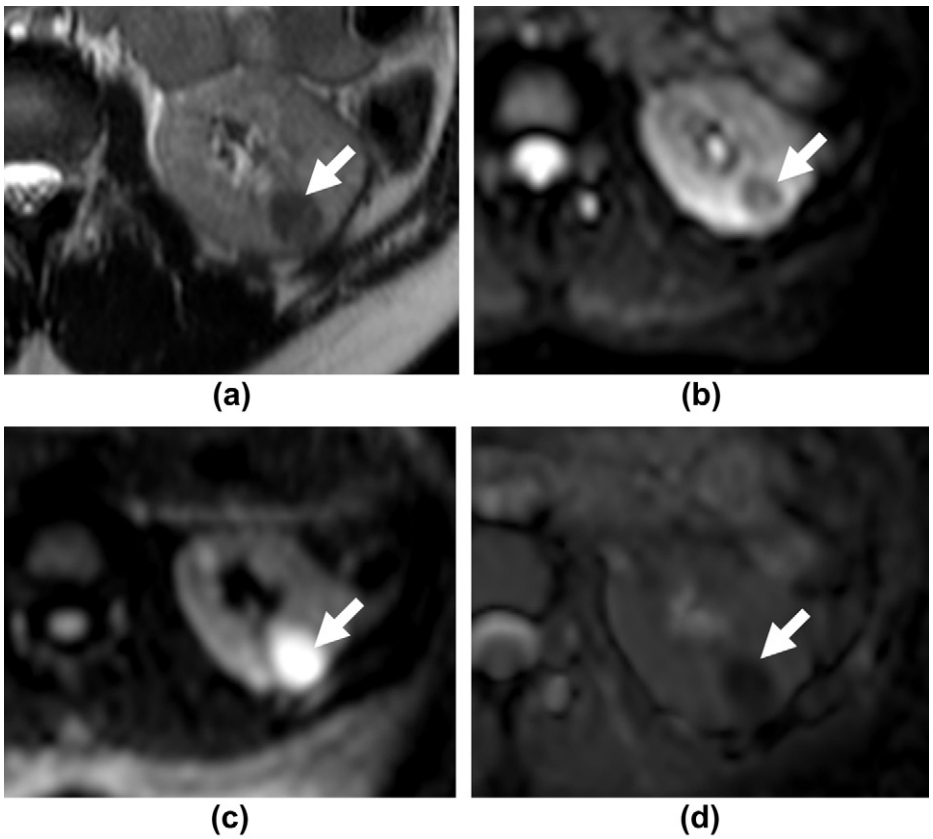


**Figure 6** Minimal fat AML in a 28-year-old man. (a) Axial T2-weighted image shows a slightly and heterogeneously hypointense lesion (arrow). (b, c) Axial diffusion-weighted images with b values of 0 (b) and 1000 (c) s/mm$^2$: the lesion is hypointense at b0 s/mm$^2$ and hyperintense at b 1000 s/mm$^2$. (d) Corresponding ADC map shows a lesion that is hypointense to uninvolved kidney. Lesion ADC is $1.04 \times 10^{-3}$ mm$^2$/s. Kidney ADC is $1.98 \times 10^{-3}$ mm$^2$/s. This case underlines the observation that hypointensity on the ADC map and low ADC value are not imperatively associated with malignancy.

overlaps among ADC values of small solid renal masses occur, DWI cannot be used as a standalone sequence for lesion characterization, and ADC values should be concurrently interpreted with all available images to avoid misinterpretation.

## References


1. Berland LL, Silverman SG, Gore RM, et al. Managing incidental findings on abdominal CT: white paper of the ACR incidental findings committee. *J Am Coll Radiol* 2010;**7**:754–73.
2. Silvermann SG, Israel GM, Herts BR, et al. Management of the incidental renal mass. *Radiology* 2008;**249**:16–31.
3. Frank I, Blute MI, Cheville JC, et al. Solid renal tumors: an analysis of pathological features related to tumor size. *J Urol* 2003;**170**: 2217–20.
4. O'Connor SD, Pickhardt PJ, Kim DH, et al. Incidental finding of renal masses at unenhanced CT: prevalence and analysis of features for guiding management. *AJR Am J Roentgenol* 2011;**197**:139–45.
5. Li Guorong, Cuilleron M, Gentil-Perret A, et al. Characteristics of image detected solid renal masses: implication for optimal treatment. *Int J Urol* 2004;**11**:63–7.
6. Ljungberg B, Cowan NC, Hanbury DC, et al. EAU guidelines on renal cell carcinoma: the 2010 update. European Association of Urology Guideline Group. *Eur Urol* 2010;**58**:398–406.
7. Scialpi M, Di Maggio A, Midiri M, et al. Small renal masses: assessment of lesion characterization and vascularity on dynamic contrast-enhanced MR imaging with fat suppression. *AJR Am J Roentgenol* 2000;**175**:751–7.
8. Pedrosa I, Sun MR, Spencer M, et al. MR imaging of renal masses: correlation with findings at surgery and pathologic analysis. *RadioGraphics* 2008;**28**:985–1003.
9. Dyer R, Di Santis DJ, McClennan BL. Simplified imaging approach for evaluation of the solid renal mass in adults. *Radiology* 2008;**247**:331–43.
10. Sun MR, Ngo L, Genega EM, et al. Renal cell carcinoma: dynamic contrast-enhanced MR imaging for differentiation of tumor subtypes—correlation with pathologic findings. *Radiology* 2009;**250**: 793–802.
11. Choudhary S, Rajesh A, Mayer NJ, et al. Renal oncocytoma: CT features cannot reliably distinguish oncocytoma from other renal neoplasms. *Clin Radiol* 2009;**64**:517–22.
12. Kim JI, Cho JY, Moon KC, et al. Segmental enhancement inversion at biphasic multidetector CT: characteristic finding of small renal oncocytoma. *Radiology* 2009;**252**:441–8.
13. Verma SK, Mitchell DG, Yang R, et al. Exophytic renal masses: angular interface with renal parenchyma for distinguishing benign from malignant lesions at MR imaging. *Radiology* 2010;**255**:501–7.
14. Scialpi M, Cardone G, Barberini F, et al. Renal oncocytoma: misleading diagnosis of benignancy by using angular interface sign at MR imaging. *Radiology* 2010;**257**:587–8.
15. Millet I, Doyon FC, Hoa D, et al. Characterization of small solid renal lesions: can benign and malignant tumors be differentiated with CT? *AJR Am J Roentgenol* 2011;**197**:887–96.
16. Henderson RJ, Germany R, Peavy PW, et al. Fat density in renal cell carcinoma: demonstration with computerized tomography. *J Urol* 1997;**157**:1347–8.
17. Rosenkrantz AB, Hindman N, Fitzgerald EF, et al. MRI features of renal oncocytoma and chromophobe renal cell carcinoma. *AJR Am J Roentgenol* 2010;**195**:W421–7.

18. Kim S, Jain M, Harris AB, et al. T1 hyperintense renal lesions: characterization with diffusion-weighted MR imaging versus contrast-enhanced MR imaging. *Radiology* 2009;**251**:796–807.
19. Taouli B, Thakur RK, Mannelli L, et al. Renal lesions: characterization with diffusion-weighted imaging versus contrast-enhanced MR imaging. *Radiology* 2009;**251**:398–407.
20. Wang H, Cheng L, Zhang X, et al. Renal cell carcinoma: diffusion-weighted MR imaging for differentiation at 3.0 T. *Radiology* 2010;**257**:135–43.
21. Squillaci E, Manenti G, Cova M, et al. Correlation of diffusion-weighted MR imaging with cellularity of renal tumours. *Anticancer Res* 2004;**24**:4175–9.
22. Paudyal B, Paudyal P, Tsushima Y, et al. The role of the ADC value in the characterisation of renal carcinoma by diffusion-weighted MRI. *Br J Radiol* 2010;**83**:336–43.
23. Razek AA, Farouk A, Mousa A, et al. Role of diffusion-weighted magnetic resonance imaging in characterization of renal tumors. *J Comput Assist Tomogr* 2011;**35**:332–6.
24. Cova M, Squillaci E, Stacul F, et al. Diffusion-weighted MRI in the evaluation of renal lesions: preliminary results. *Br J Radiol* 2004;**77**:851–7.
25. Le Bihan D. Intravoxel incoherent motion imaging using steady-state free precession. *Magn Reson Med* 1988;**7**:346–51.
26. Wagner BJ, Wong-You-Cheong JJ, Davis Jr CJ. Adult renal hamartomas. *RadioGraphics* 1997;**17**:155–69.
27. Prasad SR, Humphrey PA, Catena JR, et al. Common and uncommon histologic subtypes of renal cell carcinoma: imaging spectrum with pathologic correlation. *RadioGraphics* 2006;**26**:1795–806.
28. Amin MB, Crotty TB, Tickoo SK, et al. Renal oncocytoma: a reappraisal of morphologic features with clinicopathologic findings in 80 cases. *Am J Surg Pathol* 1997;**21**:1–12.
29. Zhang JL, Sigmund EE, Chandarana H, et al. Variability of renal apparent diffusion coefficients: limitations of the monoexponential model for diffusion quantification. *Radiology* 2010;**254**:783–92.
30. Blackledge MD, Leach MO, Collins DJ, et al. Computed diffusion-weighted MR imaging may improve tumor detection. *Radiology* 2011;**261**:573–81.